DESIGN AND ANALYSIS OF A COUNTERTOP MEAT DEFROSTER

Thomas Anderson, Jaydutt Kulkarni, Benjamin York
thomasa1, jkulkarn, byork

ABSTRACT

In this report, we propose and simulate a countertop meat defrosting device based on the coupling of conduction, forced convection and phase change. The overall targets of the proposed defroster device are to raise the minimum temperature of the meat to 0ºC while not allowing the maximum temperature along the meat surface to exceed room temperature. These targets are to be achieved in a timeframe comparable to benchmarked commercial devices available in the market, while providing compactness and ease of use.

The dimensions of the device were primarily dictated by the need to have a countertop device, which is why a kitchen microwave was chosen as a benchmark. The geometry of the device and meat were generated using SpaceClaim, imported into ANSYS Workbench and then meshed using relevant techniques to ensure a good quality grid. Using turbulent flow of air forced into the device via a fan, the setup was simulated in ANSYS Fluent for different material properties until an operating solution was found. The results of the simulation were then compared with the performance of commercially available devices to assess viability.

INTRODUCTION AND BACKGROUND

Meat is among the most perishable food items, yet 10 - 20% of calories consumed per day world-wide come from meat. Until recently, this figure continually rose. Now, the amount of meat eaten per person per day has become relatively stable. The ability to preserve and transport meat may be a contributing factor to bringing these numbers up in areas where grain and produce have traditionally been the primary sources of nutrition [1]. As development in preservation techniques advanced over the course of centuries, freezing became the most common method for preserving freshly butchered meat. Freezing meat has the benefit of inhibiting the microbial spoilage that can occur above -12°C. It is possible, however, that the act of freezing and thawing itself can deteriorate the fibers of meat. It is a current concern that meat that is being eaten is of the same quality as when it is initially frozen [2].

The preservation of meat has allowed for a much increased shelf life, resulting in the ability to transport this meat over greater distances from where it originated. As a result, many people around the world rely on frozen meat to fulfill their dietary needs. A common problem among household chefs is the issue of preparing frozen meat. The problem isn't so much the actual cooking of this meat, but safely and quickly thawing it. The vast majority of meat cooked in households across the world have been frozen prior to preparation. Since the beginning of this practice, chefs have had to plan ahead and properly time how long it might take for their meat to reach an appropriate temperature. In recent years, defrosters have been developed for restaurant and large-scale use in order to cut down the time and effort in food preparation. This work aims to develop a product that may bring this convenience to the kitchens of those who only need to prepare a small portion of frozen meat [3].

Among currently available options for household chefs are so-called "enhanced defrosting trays." These trays actually do very little to enhance natural convection to the meat aside from allowing slots for ice-melt to leave the meat. These defrosting trays require much time at room temperature for frozen meat to thaw. This leaves the meat susceptible to microbial spoilage. This method is truly no better than leaving frozen meat on a countertop overnight, which is discouraged greatly by USDA recommendation.

TABLE 1. POWER BREAKDOWN FOR ICE-OFF MACHINE [4]

Component	Power (W)
Total Power	1200
Fan Power Approximation	100
Lights and other power	200
Radiative + Conductive	900

In order to accomplish the goals of this work, various industrial scale defrosters were studied as benchmarks. Such an example is the Ice-Off defroster shown in Fig. 1. Performance in terms of meat defrosting time was available, however information regarding the methods of heat transfer employed by each was not disclosed. Table 1 provides benchmarking data for commercially available devices.

Keeping these things in mind, it is the goal of this work to develop a model that simulates the defrosting of meat. This model has a geometry that is comparable to that of an ordinary microwave oven. Using conductive and convective heat transfer, this defroster should be able to provide sufficient heating power to raise the internal temperature of a slab of meat to a fully defrosted state within a reasonable amount of time.

The thermo-physical properties of any meat will change with change in temperature. Empirical correlations developed by culinary scientists regarding changes in thermal conductivity [5], specific heat capacity [6] and density [7] of meat with respect to temperature will have to be used in order to simulate the heating conditions more accurately. Additionally, the modes of heat transfer will be affected by the changes in meat properties over time. As such, the fully developed model should be capable of incorporating these effects. In order to obtain highly accurate results, a progressive approach must be followed which slowly incorporates all types of unknowns into the setup.

PROBLEM SETUP

The problem setup has been divided into a number of sections that deal with specific aspects of each phase of simulation as well as the schematic.

FIGURE 1. ICE-OFF DEFROSTER [8]

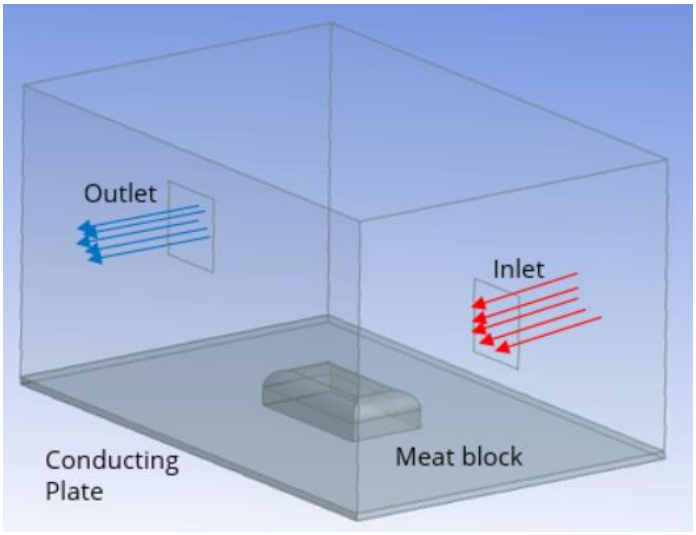

FIGURE 2. DEFROSTER SCHEMATIC

Geometry of System

Consider fluid (air) entering the domain through the inlet as shown in Fig. 2. In order to better understand the effects of conduction and convection, a meat slab was placed near the inlet on a metal (Al) plate which was supplied with heat flux. The air recirculates and provides a thawing effect to the frozen meat until the time it has gained enough temperature to rise up and escape through the outlet. The air is being forced into the domain via a fan. Throughout this investigation, the geometry of the enclosure, including inlet, outlet, and plate thickness are to remain constant while the flow and heating parameters are altered.

For the purposes of the project, the lateral walls of the plate and all the walls of the device are considered to be adiabatic. No slip condition is assumed on the walls and zero-gauge pressure condition is used for the pressure outlet. The air is assumed to be dry, i.e., there is absence of any H_2O in gaseous state in order to simplify the model.

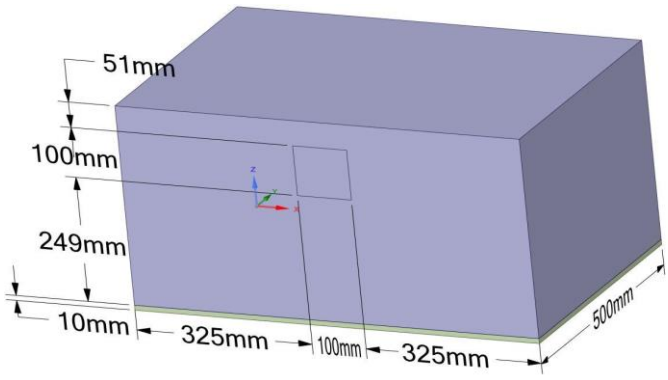

FIGURE 3. GEOMETRIC PARAMETERS OF SETUP

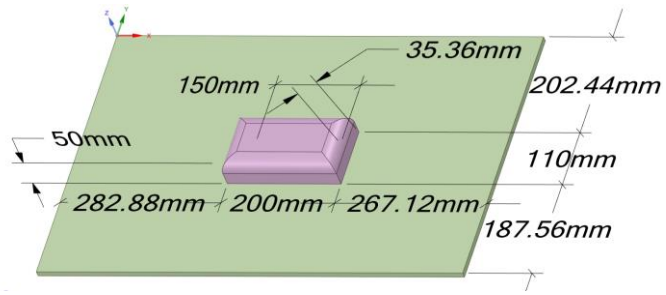

FIGURE 4. POSITION OF MEAT BLOCK

As shown in Fig. 3, the outlet is taken to be 100mm x 100m in dimension, the same as the inlet. The inlet is placed 30mm above ground level while the outlet is placed 250mm above ground level, where ground level is the top surface of the conducting plate. Overall dimensions of the device are 750mm x 500mm x 400m with a conducting plate of thickness 10mm. The meat block is approximately 1100 mm^3 in volume and is purposely placed at an asymmetric location on the plate in order to simulate real-world conditions, as shown in Fig. 4. The meat block profile used is that of a cuboid with the upper edges filleted. This is to ensure a good quality mesh and a simplified geometry to understand temperature distribution. Throughout this investigation, the geometry of the enclosure, including inlet, outlet, and plate thickness are to remain constant while the flow and heating parameters are altered.

Meshing of System

Since the only component in the system that was sweepable was the conducting plate, the entire domain was meshed using tetrahedral cells to maintain uniformity and reduce skewness. As shown in Fig. 5, the area near the block of meat was meshed using finer grid while that away from the meat was meshed using a coarser grid.

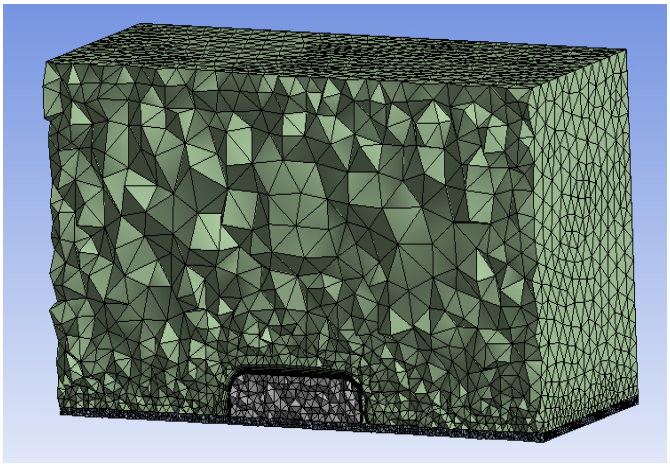

FIGURE 5. CROSS-SECTION OF MESHED DOMAIN

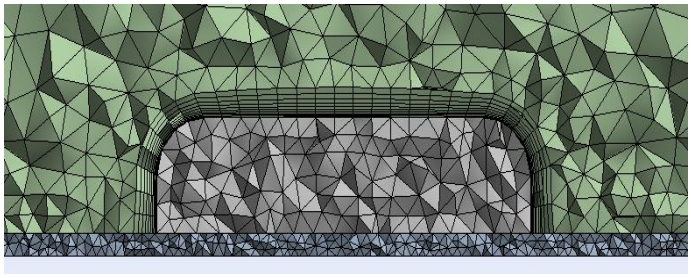

FIGURE 6. NEAR-WALL MESH

Meshing was done using the parameters defined in Table 2. The key parameters to monitor were the number of elements and the maximum skewness. Due to computational cost associated with increasing the number of elements, meshing had to be done in such a way that the number of elements in the domain was limited to less than 10^6. The maximum skewness in the grid was also monitored to ensure that it does not become greater than 0.8, which is an empirical criteria used to ensure solution convergence. The inflation layer was initially applied to both the meat and the conducting plate, but due to the maximum skewness of the grid exceeding 0.9, it was limited to just the meat block, as shown in Fig. 6.

Model Simulations

For the early portion of this work, the frozen meat was designated as a solid with constant properties. This simplification was necessary to begin understanding how different modes of heat transfer would affect the temperature distribution early on in the defrosting process. As this investigation progressed through the geometry creation stages, it was evident that simulating the entire defrosting process needed to be broken down into several distinct steps. Each step will provide further insight into the behavior of the model and help tweak the parameters to achieve optimum thawing conditions. Starting with a steady state solution, with steady progression into transient flow models and finally into a phase-change accommodated simulation, there were clear takeaways regarding the range of heat flux and the range of inlet air velocity required to operate the device.

TABLE 2. MESH PARAMETERS

Parameter	Value
Number of nodes	91611
Number of elements	401250
Global element size	2.5mm
Plate element size	5mm
Maximum skewness	0.63874
Average skewness	0.2639
Inflation growth rate	1.2
Inflation layers	10
Transition ratio	0.272

Step 1: Steady State Simulation (Solid-Phase Meat)

In order to validate the model that was created, it was necessary to simulate a steady state solution. From this, it was possible to see that the solution was converging. Not only was it seen that the model was usable, but it was also possible to gain some insight as to the expected performance that would be achieved if the simulation was ever to reach a steady state in the real world. The results of such simulations are discussed at greater length in later sections of this paper.

Step 2: Transient Simulation (Solid-Phase Meat)

After validating the model through the use of the steady state simulation, a transient simulation was attempted. This method uses the same constant property meat block as the steady state trials. The difference is that now the simulation provides data regarding the temperature distribution at a desired time step. Within this step, a study was conducted to ensure that the chosen time step was small enough to provide accurate results without becoming too computationally expensive. Once this time step was decided upon, it was possible to run full-length simulations over the duration that was chosen. By iteratively changing the parameters that affect heat transfer to the meat, it is possible to ascertain which range of each value may be conducive to recreating competitive defrosting performance when compared to the benchmark values.

Step 3: Simplified Phase Change Simulation

The previous steps simplify the heat transfer through the block of meat by assuming constant properties and state. However to represent the real world defrosting of meat not only do you need to change the properties, but the latent heat of melting adds another element that we need to model. As such, we created a separate simulation with only ice and applied a heat flux to the bottom of that block. This simplest of possible melting models allowed us to determine that the phase change of any material could be modeled based on properties that we provided.

Step 4: Transient Simulation (Solid-Phase Meat)

Using the model tested in *Step 2*, along with the addition of a bottom metal plate from the defroster, the material properties of the meat, i.e., thermal conductivity, specific heat capacity and density, were varied according to changing temperature of the meat block. Since the time step is already determined, and a range of heat flux values and air velocity values are to be tested, piecewise functions were used instead of constant material properties. Empirical relations between mass fractions of protein, ice, water and fat were utilized to establish properties of meat at all temperatures in the operating range. Using chicken as our type of meat, we have:

Thermal conductivity below freezing point (0 ^{o}C):

$$k = 2.472X_W + 0.00998(X_P/X_F) - 0.00346T - 0.611 \quad (1)$$

Thermal conductivity above freezing point:

$$k = 0.476 + 0.000605T \quad (2)$$

Specific heat capacity:

$$Cp = 4.18X_W + 1.711X_P + 1.928X_F \quad (3)$$

Density:

$$\rho = \frac{(1-\varepsilon)}{\Sigma\frac{X_i}{\rho_i}} \quad (4)$$

Step 5: Transient Simulation (Phase-Changing Meat)

Due to the limitations of the melting/solidification model the full domain model could not be integrated with a phase change component because of the reactionary flow surrounding the melting meat block. Therefore, we approached it using a two-fold method: (1) we determined a time and surface averaged convection coefficient at the surface of the meat block, (2) this value is then applied to the surface of the meat in the simplified meat phase change model. The result from this model showed some correlation with the real world data we collected from our Ice-Off competitors. Once we had shown this simplified method for coupling two models was reasonably accurate, we proceeded to expand upon this principle.

In order to provide a more exact result, we collected a convection coefficient value at every three time steps during the full domain simulation using a representative meat block. This time step value for convection coefficient was then fit with a line of best fit for the first half of the data while it was more linear. Another line of best fit was fitted to the second half of data to get the closest overall expression for the convective coefficient of the surface of the meat. The two expressions were applied to the simplified model using an IF boundary condition and swapping expressions at a point where the h values in the simulation began spiking. The results from this model were then used as our final comparison to the Ice-Off data.

NUMERICAL FORMULATION

Since the air inlet acts as a jet flow, the numerical scheme will be decided based on Reynolds number which will determine the nature of the flow. During the simulation phase, an air velocity of 8 m/s was determined to be optimal for thawing the meat. So, the Reynolds number based on this air velocity and properties of air at room temperature:

$$Re = \frac{\rho u D_h}{v} \quad (5)$$

For the setup, u = 8 m/s and D_h = 0.1m

For air at 300K,
$\rho = 1.61\ \text{kg/m}^3$ and $\upsilon = 1.846\text{e} - 5\ \text{kg/m} - \text{s}$

For the jet flow, Re = 69772.48 (>2000, turbulent flow)

Using empirical relationship between turbulence intensity and Reynolds number:

$$I = 0.16(Re)^{\frac{-1}{8}} \quad (6)$$

From this, turbulence intensity is given as I = 3.968% ~ 4%

Since we are dealing with turbulent flow, a Reynolds-averaged-Navier-Stokes (RANS) model was used for simulating all transient phases. Time-dependent solutions of the Navier-Stokes equations for high Reynolds-number turbulent flows in complex geometries which set out to resolve all the way down to the smallest scales of the motions are unlikely to be attainable for some time to come. Two alternative methods can be employed to render the Navier-Stokes equations tractable so that the small-scale turbulent fluctuations do not have to be directly simulated: Reynolds-averaging (or ensemble-averaging) and filtering. Both methods introduce additional terms in the governing equations that need to be modeled in order to achieve a "closure" for the unknowns. RANS equations govern the transport of the averaged flow quantities, with the whole range of the scales of turbulence being modeled [9]. The closure model used for RANS is the k-omega (k-ω) turbulence model to simulate mean flow characteristics for turbulent flow conditions. It is a common two-equation turbulence model that attempts to predict turbulence by two partial differential equations for two variables, k and ω. The first variable k represents the turbulent kinetic energy while the second variable ω represents the specific rate of dissipation of the turbulent kinetic energy into internal thermal energy [10].

The shear-stress transport (SST) k-ω model effectively blends the robust and accurate formulation of the k-ω model in the near-wall region with the free stream independence of the k-ε model in the far field. To achieve this, the k-ε model is converted into a k-ω formulation. The SST k-ω model is similar to the standard k-ω model, but includes the following refinements:

- The standard k-ω model and the transformed k-ε model are both multiplied by a blending function and both models are added together. The blending function is designed to be one in the near-wall region, which activates the standard k-ω model, and zero away from the surface, which activates the transformed k-ε model.
- The SST model incorporates a damped cross-diffusion derivative term in the ω equation.
- The definition of the turbulent viscosity is modified to account for the transport of the turbulent shear stress.
- The modeling constants are different.

These features make the SST k-ω model more accurate and reliable for a wider class of flows (e.g., adverse pressure gradient flows, airfoils, transonic shock waves) than the standard k-ω model. Other modifications include the addition of a cross-diffusion term in the ω equation and a blending function to ensure that the model equations behave appropriately in both the near-wall and far-field zones. The transport equations for the SST k-ω model are given as:

$$\frac{\partial(\rho k)}{\partial t} + \frac{\partial(\rho k u_i)}{\partial x_i} = \frac{\partial}{\partial x_j}\left(\Gamma_k \frac{\partial k}{\partial x_j}\right) + \widetilde{G_k} - Y_k + S_k \quad (7)$$

$$\frac{\partial(\rho \omega)}{\partial t} + \frac{\partial(\rho \omega u_i)}{\partial x_i} = \frac{\partial}{\partial x_j}\left(\Gamma_\omega \frac{\partial \omega}{\partial x_j}\right) + \widetilde{G_\omega} - Y_\omega + S_\omega + D_\omega \quad (8)$$

The spatial numerical scheme chosen was the Coupled algorithm. The pressure-based solver allows you to solve your flow problem in either a segregated or coupled manner. Using the coupled approach offers some advantages over the non-coupled or segregated approach. The coupled scheme obtains a robust and efficient single phase implementation for steady-state flows, with superior performance compared to the segregated solution schemes. This pressure-based coupled algorithm offers an alternative to the density-based and pressure-based segregated algorithm with pressure-velocity coupling. For transient flows, using the coupled algorithm is necessary when the quality of the mesh is poor, or if large time steps are used. The pressure-based segregated algorithm solves the momentum equation and pressure correction equations separately. This semi-implicit solution method results in slow convergence. The coupled algorithm solves the momentum and pressure-based continuity equations together. The full implicit coupling is achieved through an implicit discretization of pressure gradient terms in the momentum equations, and an implicit discretization of the face mass flux.

While the primary model for the project was being modeled using classic fluid dynamics models. However this project also required some of the more specialized capabilities available in ANSYS Fluent, specifically the built-in capabilities for dealing with the melting and solidification of materials. This model represents the material using an enthalpy-porosity formulation, where the temperature change of the material is modeled using the specific heat in each cell plus the latent heat capacity ($H = h + \Delta H$).

There is also a built in momentum sink to deal with the volume and pressure change due to a transition from solid to liquid. For example in our model the meat melts and becomes more dense, however since the overall size and volume are constant the momentum sink is able to account for that incongruity. However, when there is a change from solid to liquid the porosity of the material is zero which does not allow for velocities in this region. Therefore the momentum sink in this

"mushy zone" takes on the below form. εrepresents 0.001 or an equally small number so that there is no division by zero when the momentum is being solved for in a solid region.

$$S = \frac{(1-\beta)^2}{(\beta^3-\varepsilon)} A_{mush}(v - v_p) \quad (9)$$

The second main component of this model is that it does not track the interface between solid and liquid, but instead it determines the liquid fraction in each cell using the enthalpy equation listed above. So the simplest approximation that the solver can use for liquid fraction (β) inside each cell is a linear interpolation of the solidus, liquidus, and current temperature.

$$\beta = \frac{T - T_{solidus}}{T_{liquidus} - T_{solidus}} \quad (10)$$

Lastly the solidification/ melting model has some limitations in how it can be used in Fluent modeling. First the melting/solidification model cannot be used in conjunction with any reacting flow as we discovered when attempting to integrate it into our complete fluid domain. Secondly, the melting and solidification solver only works with segregated solvers and does not work with the coupled solver. So the formulation for the entire fluid domain combined with the phase change was switched to a PISO solver so that the melting/solidification model could be added. The PISO solver was included because as the model runs each time step the momentum calculations, which we described the importance of earlier, are done iteratively multiple times during each iteration. While this increases the time to complete each iteration it lowers the number of iterations required to converge the velocities and therefore the momentum and continuity especially in the "mushy zone."

RESULTS AND DISCUSSION SECTION

Due to the fact that this investigation had several distinct steps that each concluded with useful information, we have split each trial's results up accordingly. In this manner, they may be better understood and important results can be correlated with each other effectively.

Step 1: Steady State Simulation (Solid-Phase Meat)

The results from carrying out a steady state solution are not so much quantitative in their importance, but more qualitative. The simulation showed that the developed model had the capability of being implemented in a more complicated transient simulation from which data could be analyzed. The residuals from such a test are shown in Appendix A, Fig. A1.

It is possible to see that the entire block of meat rises to temperatures much higher than those desired for the purpose of only defrosting the meat. This is also shown in Appendix A, Fig. A2. This result occurred whether extremely low/negligible heat flux or a massive heat flux was applied through the bottom plate. From this, it was deduced that a steady state condition should actively be avoided. Additionally, it would take much longer than the targeted time range to actually reach this steady state condition. For the purposes of this project, it was deemed unwise to run transient solutions to the extent of reaching steady state for the sake of computational expense and lack of information that this would provide. Taking the information that we had gained, however, it was possible to confidently move forward with the investigation.

Step 2: Transient Simulation (Solid-Phase Meat)

The transient simulation that made use of the constant-property, solid-phase meat was the simulation that provided the most insight for this investigation. Before carrying out full length simulations, a time-step study was done. In this study, each adjustable parameter (inlet velocity, inlet temperature, and bottom plate heat flux) was held constant. The methods and controls used within the solver were also held constant, while only the size of the time step was altered.

For this study, the time step of 0.05 seconds and 0.25 seconds were tested. Each simulation was run for a flow-time of one minute, and then compared. From Appendix B, Figs. B2 & B6, it is evident that the temperature distribution throughout the slab of meat is nearly identical for each trial. The differences between the two trials were apparent when analyzing the velocity distribution throughout the enclosure. For the sake of this project, it was decided to neglect these differences. It is true, however, that a change in velocity profile near the surface of the meat may have a significant effect on the convective heat transfer coefficient, and thus an effect on the amount of heat that can realistically enter through the meat's surface.

Regardless, the larger time step of 0.25 second was chosen for the remainder of the trials. It was evident through the time-step study that the heat transfer from convection through the surface should remain roughly equivalent despite these velocity effects. Additionally, the investigation was not as concerned with the complex behavior of the air flowing throughout, rather the temperature distribution was the focal point of the project. This allowed for more trials to be carried out, allowing for an iterative process in which the parameters that resulted in the most desirable performance could be obtained.

Using this iterative method, several values for each parameter of interest were systematically implemented and evaluated. In lieu of the data for each trial, a map showing relative performance is displayed in Fig. 7. It is apparent that the inlet velocity and imposed heat flux on the bottom plate were changed. Temperature is neglected in this figure, as it was found that the inlet air's temperature had only a minor effect on the overall performance of the system when compared to changes in the velocity and heat flux. Each trial within the study shown had inlet air temperature designation of 300 K.

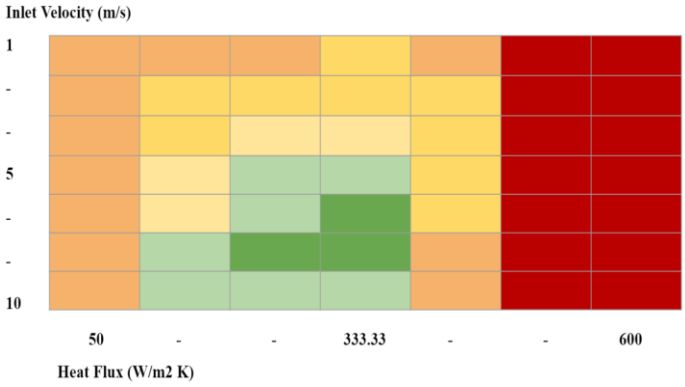

FIGURE 7. PARAMETER OPTIMIZATION

It is important to note that a trial was not carried out for each individual box as shown in the figure, but several trials had been conducted among the team at various extremes within the range shown on the figure. A consensus was reached as far as the optimal range that could be found through this iterative method.

Using this method, we found that the range for optimal inlet velocity and applied heat flux to be ~8m/s and ~333.33 W/m2 respectively. These values are then used to carry out the full-length transient simulation in which the convective heat transfer coefficient is found. The convective heat transfer coefficients found are then implemented in the Simplified Phase Change Simulation.

Step 3: Simplified Phase Change Simulation

During the design of the simplified phase change model it was important to first quantify the abilities of ANSYS Fluent in representing the change and then implement that to represent our meat test subject. So the first results came from modeling a simple block of ice in Fluent and changing the entire body from solid to liquid.

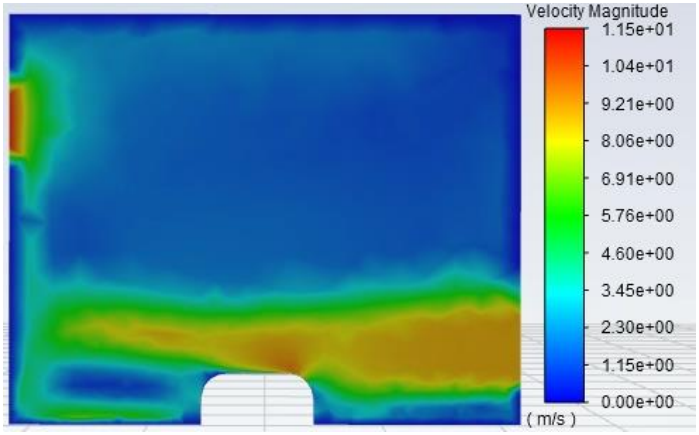

FIGURE 8. LATERAL VELOCITY PROFILE

This first test was successful after applying a density, specific heat, thermal conductivity, heat of fusion, solidus temperature, and liquidus temperature. At this stage all parameters were constant, while the last two represented what temperature the material began to freeze or melt respectively. So, by applying a simple heat flux boundary condition to the bottom surface of the ice block we were able to show the baseline capability of this solidification/melting model.

Step 4: Transient Simulation (Solid-Phase Meat)

The next step in the process was to create parameters that would change as the temperature increased in the material. Using our reference material we were able to determine exact temperature dependent properties for different kinds of meat and use those to create the material properties in Fluent. This was an important difference especially at the point of phase change because the properties would often drastically change as the meat transitioned from ice crystals to water. As can be seen in Fig. 9, we can obtain a reasonable temperature distribution before adding another layer of complexity to the model. The maximum temperature reached by the meat is around 10 ^{o}C, while the minimum temperature inside the meat is 0 ^{o}C.

The last step was to create the bottom plate of the meat defroster and integrate that with the phase change model so that any interface difficulties between the fluid representing the meat and the solid plate could be fixed. The interface had to be coupled and a heat flux was applied to the bottom of the plate and a heat flux was also applied to the air adjacent faces of the meat. As seen in Fig. 8, the resulting velocity profile is as expected, with the turbulent flow of air allowing more interaction of air at room temperature with meat at lower temperature.

Overall the proof of concept work on the phase changing capabilities proved successful and we were able to determine that Fluent could provide the resources we needed to complete this investigation into meat defrosting.

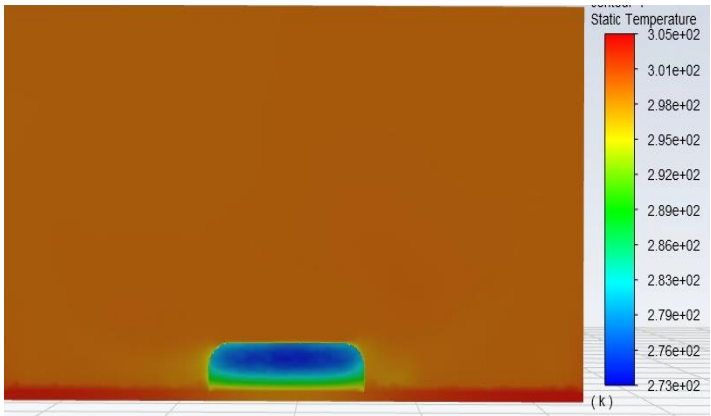

FIGURE 9. TEMPERATURE DISTRIBUTION

Step 5: Transient Simulation (Phase-Changing Meat)

The last stage of our meat defrosting investigation consisted of coupling the simple phase change model with the full defroster domain model. For this to happen, particular results for heat transfer to the meat from the surroundings within the enclosure were needed. Making use of the tools within ANSYS Fluent, it was possible to do just this. By creating a report definition, the convective heat transfer coefficient could be specified as an area-weighted average over the surface of the meat slab. An ordered list was then made, adding a value for each time step that the transient simulation was active for. By using these values, it was then possible to correlate the heat transfer properties resulting from air flow within the enclosure for the case of the solid-phase meat to the separate model which demonstrates phase change within the meat. These resultant h values after applying linear lines of best fit, ranged between 21 at the very beginning up to 300 by the end of the simulation.

Then once these values were applied to the simplified phase change model, we were able to get our final results. These final results were based on the optimal air flow and heat flux determined earlier in the process, which showed that our device has strong possibilities for use in the real world. We were able to fully defrost the meat in 10.5 minutes (**Figure C1 & C2)** and achieved a temperature of 272K throughout the meat after only 7.125 minutes (**Figure C3)**. This result meets and even exceeds that of our Ice-Off competitors which gives us the information we need to be confident moving forward with this project to a prototyping stage and testing in the real world to compare against our models.

We believe this validates our design because by using less power, less complexity, and a smaller form factor, we were able to achieve comparable results to the current market devices.

SUMMARY AND CONCLUSIONS

Throughout this work, a logical progression of steps towards developing an effective defrosting model is shown. Each of these steps provided important information that could be carried through to the next. Using the values for each parameter found through the earlier work, we found that the temperature distribution remained within a desirable range. From here, the convective heat transfer coefficients were found for each time step, and then implemented in a simplified model that consisted of only the meat and the heated plate beneath it. This meat slab was modelled using phase change, so that a higher level of insight may be gained as to the defrosting nature of frozen meat.

Important takeaways at the end of this exercise:

- There is a lot of room for differences in how the model reacts due to the complex nature of meat and the variability in how it can be modeled
- ANSYS Fluent is still limited in very specific applications such as our phase change model and may require a model that does not exactly represent the physical world in order to get an accurate result
- When creating the enclosure in which the meat slab will be placed, it may be beneficial to consider designs that direct the flow of inlet air directly to the meat. By reshaping the interior of the enclosure, it would be possible to have more control over the velocity distribution and flow patterns that will affect the rate at which heat is transferred to the meat.
- A "Design of Experiment" process can be followed to determine a series of parameter combinations that would allow for a more precise range that will grant better performance.
- The last area where the overall model can be improved is the integration of the phase change model with the overall domain model. By adding a thin solid shell separating the two fluid domains it should be possible to run the entire model. This would give us the most precise results as we wouldn't have to rely on a line of best fit in order to get exact heat transfer results on the surface of the meat.
- Proof of concept for a kitchen countertop defroster device has been validated through this exercise. With rigorous testing and more precise parametric studies, it should be possible to design a device capable of delivering a defrosting performance, in line with market expectations.

REFERENCES

1. A. Lianou and K. P. Koutsoumanis, "Evaluation of the effect of defrosting practices of ground beef on the heat tolerance of listeria monocytogenes and salmonella enteritidis," 10-Mar-2009.
2. Mascheroni. R. H. Ottino. J. Calvelo. A; "A model for the thermal conductivity of frozen meat."
3. S. Akhtar, M. I. Khan, and F. Faiz, "Effect of thawing on frozen meat quality: A comprehensive ..."
4. http://ice-off.co.kr/deforsters_down/ICE%20OFF%20IOD-MP58%20Series%20Super%20Quick%20Defroster%20for%20Meat%20restaurant.pdf
5. Kumcuoglu, S., Turgut, A. and Tavman, S. (2010), "The effects of temperature and muscle composition on the thermal conductivity of frozen meats." Journal of Food Processing and Preservation, 34: 425-438
6. Sweat, V.E., Haugh, C.G. and Stadelman, W.J. (1973), "Thermal conductivity of chicken meat at temperatures between −75 and 20°C." Journal of Food Science, 38: 158.
7. Duy K. Hoang, Simon J. Lovatt, Jamal R. Olatunji, James K. Carson, "Improved prediction of thermal properties of refrigerated foods", Journal of Food Engineering, Volume 297, 2021
8. http://www.ice-off.co.kr/company.htm
9. https://www.afs.enea.it/project/neptunius/docs/fluent/html/th/node45.htm
10. https://www.afs.enea.it/project/neptunius/docs/fluent/html/th/node67.htm

NOMENCLATURE

$X_{W:}$	Mass fraction of ice/water (depending on its state)
X_P:	Mass fraction of protein
X_F:	Mass fraction of fat
T:	Temperature, in ^oC
ε:	Porosity
u:	Inlet velocity
D_h	Hydraulic diameter (Characteristic length)
u_i:	Velocity field
ρ:	Fluid density
υ:	Dynamic viscosity
$\widetilde{G_k}$:	Generation of turbulence kinetic energy due to mean velocity gradients
G_ω:	Generation of ω
Γ_k:	Effective diffusivity of k
Γ_ω:	Effective diffusivity of ω
Y_k:	Dissipation of k due to turbulence
Y_ω:	Dissipation of ω due to turbulence
D_ω:	Cross-diffusion term
S_k:	User-defined source term for k
S_ω:	User-defined source term for ω

APPENDIX A: Steady State, Pseudo-Transient Solution

(Pseudo Time Step: 0.25, Heat Flux: 200 W/m2, Inlet: 10 m/s, 310 K)

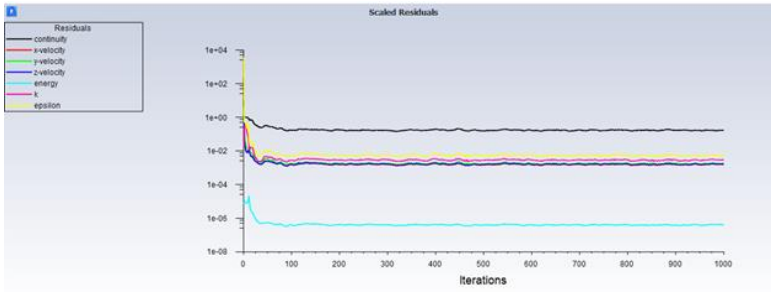

Figure A1. Residual Plot from Steady State, Pseudo-Transient Simulation

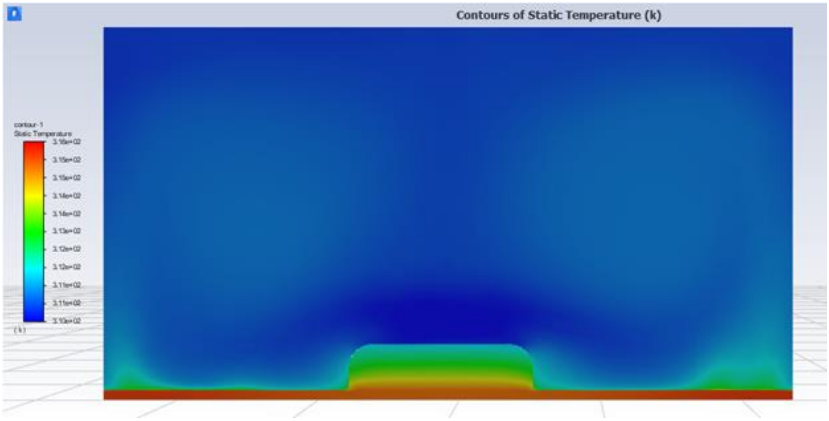

Figure A2. Temperature Distribution from Steady State, Pseudo-Transient Simulation

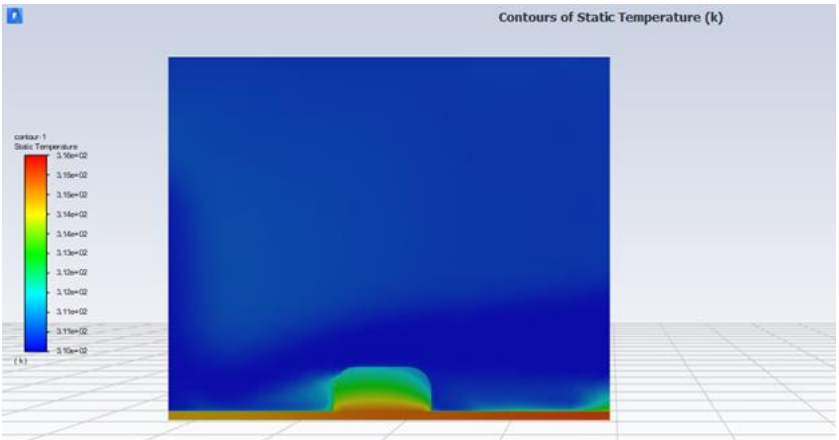

Figure A3. Temperature Distribution from Steady State, Pseudo-Transient Simulation

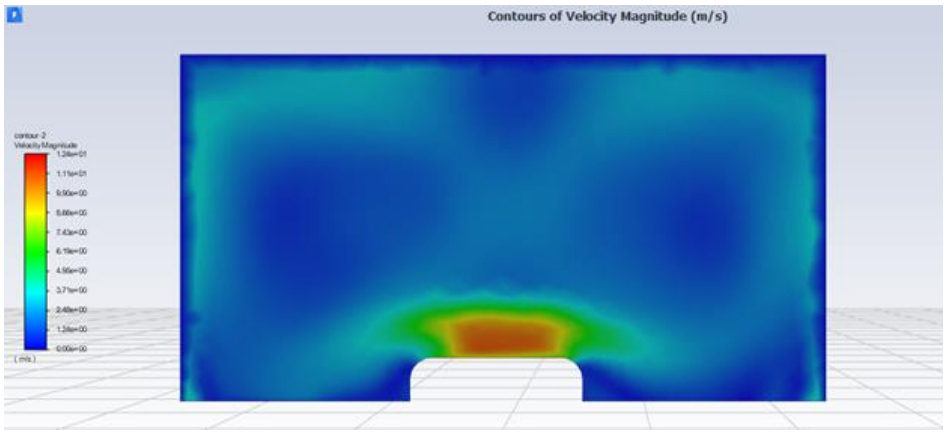

Figure A4. Velocity Distribution from Steady State, Pseudo-Transient Simulation

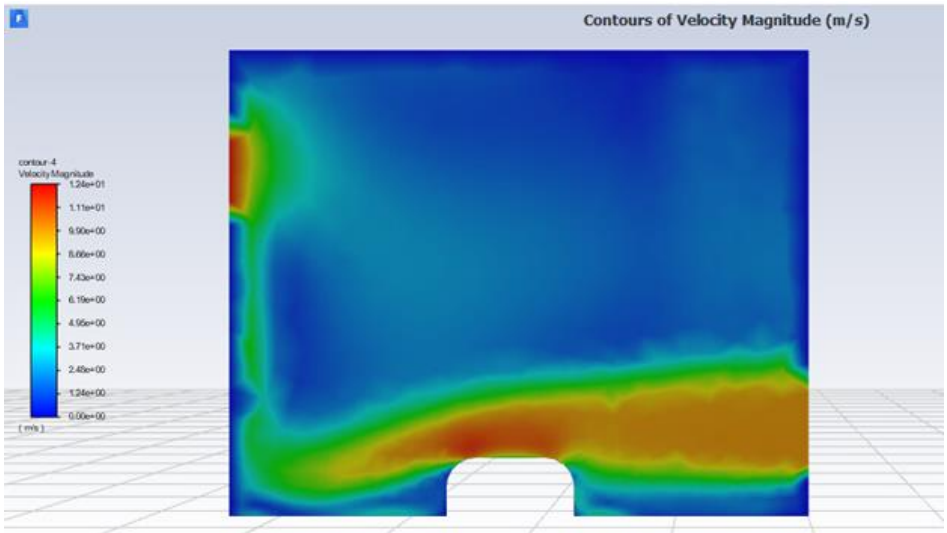

Figure A5. Velocity Distribution from Steady State, Pseudo-Transient Simulation

APPENDIX B: Time Step Convergence Study

Trial A (Run Time: 1 min, Time Step: 0.25 s, Heat Flux: 500 W/m2, Inlet: 4m/s, 300 K)

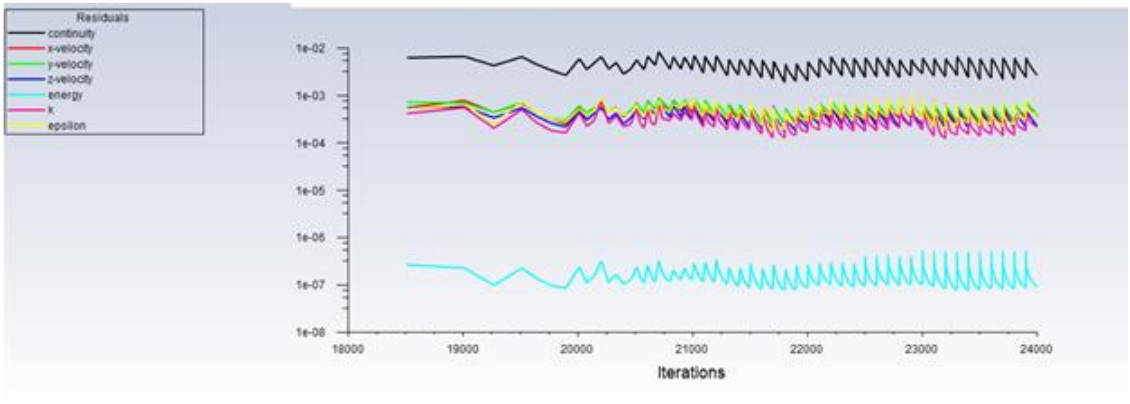

Figure B1. Residual Plot from Transient Simulation

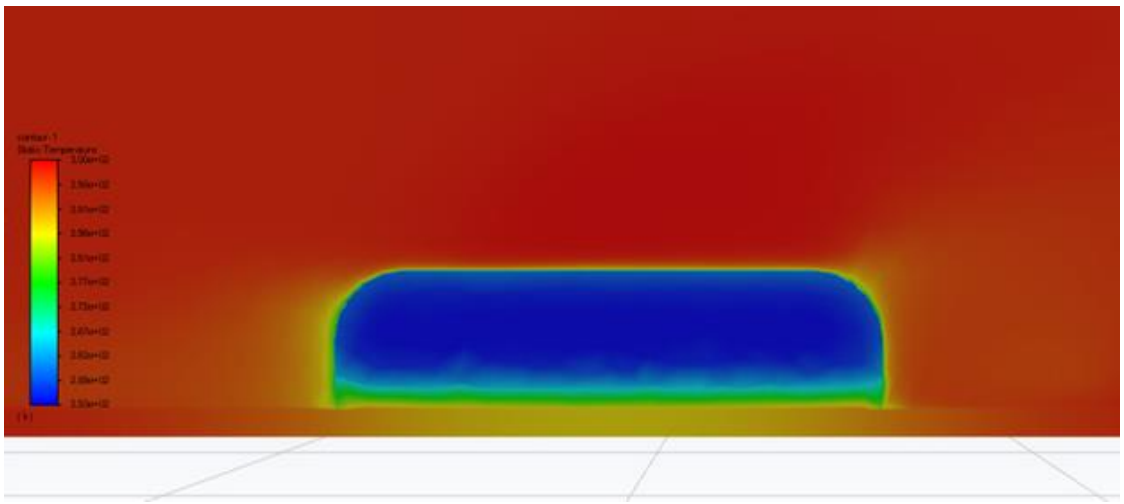

Figure B2. Temperature Distribution from Transient Simulation

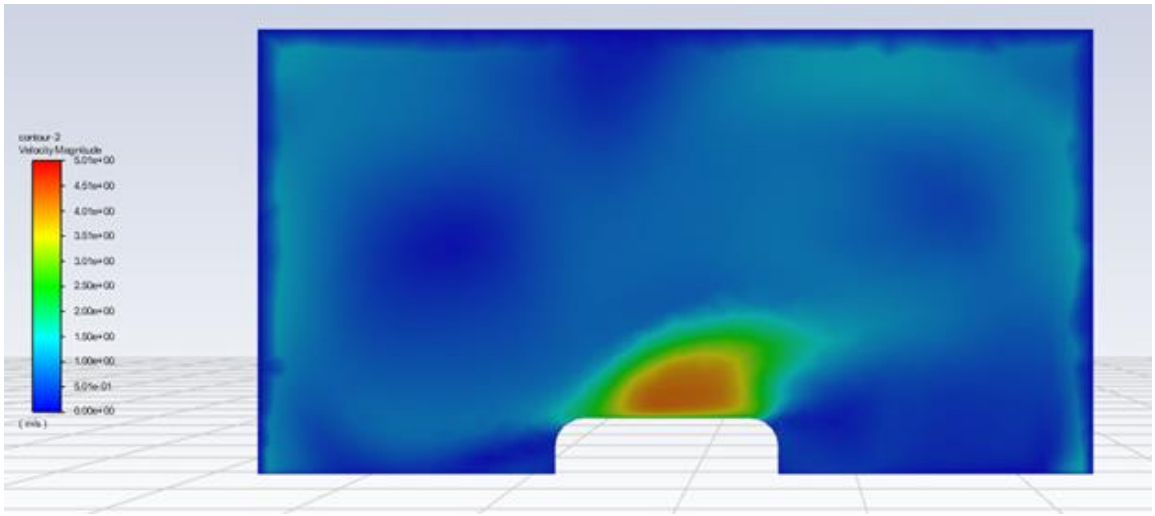

Figure B3. Velocity Distribution from Transient Simulation

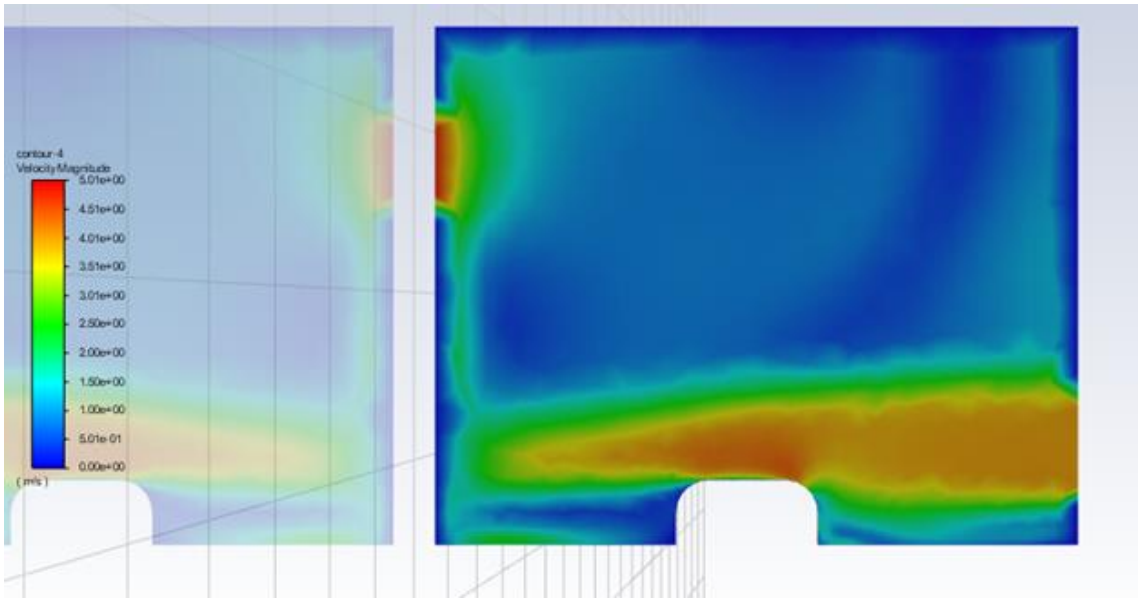

Figure B4. Velocity Distribution from Transient Simulation

Trial B (Run Time: 1 min, Time Step: 0.05 s, Heat Flux: 500 W/m2, Inlet: 4m/s, 300 K)

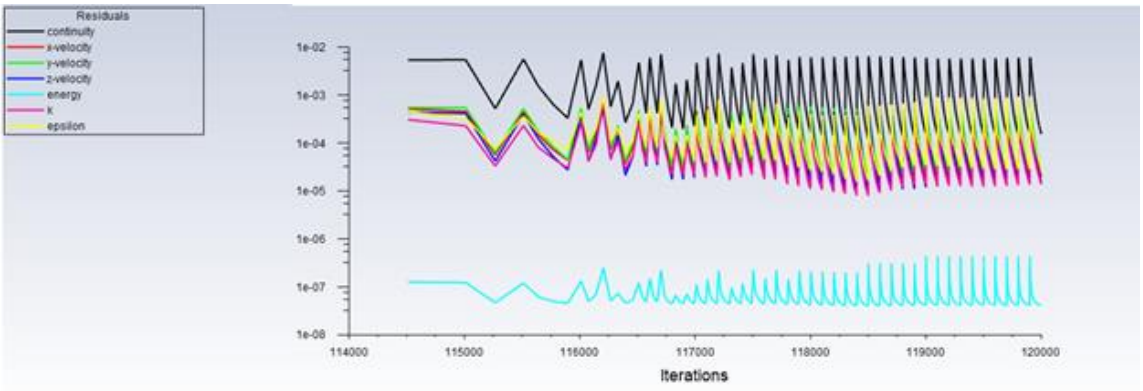

Figure B5. Residual Plot from Transient Simulation

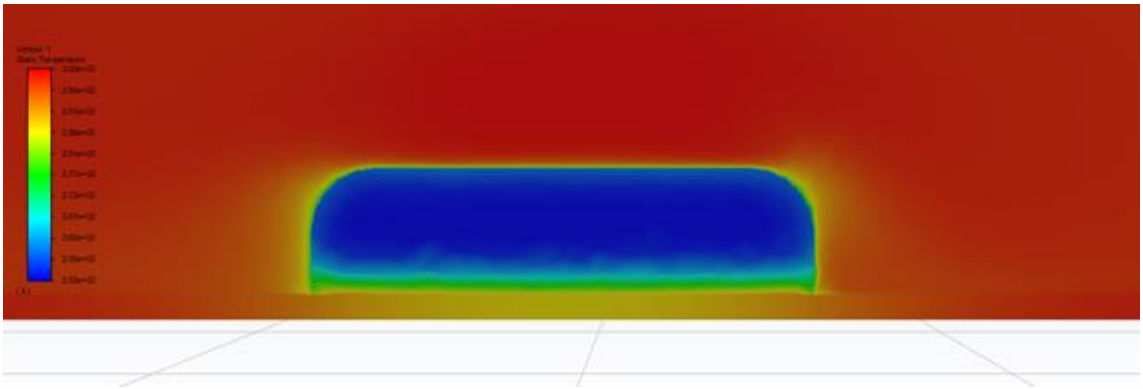

Figure B6. Temperature Distribution from Transient Simulation

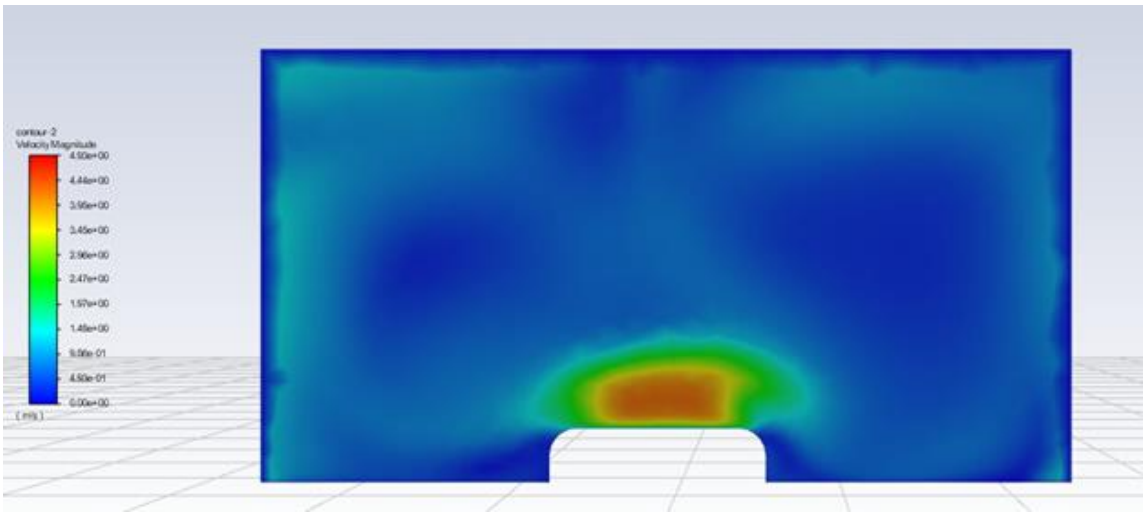

Figure B7. Velocity Distribution from Transient Simulation

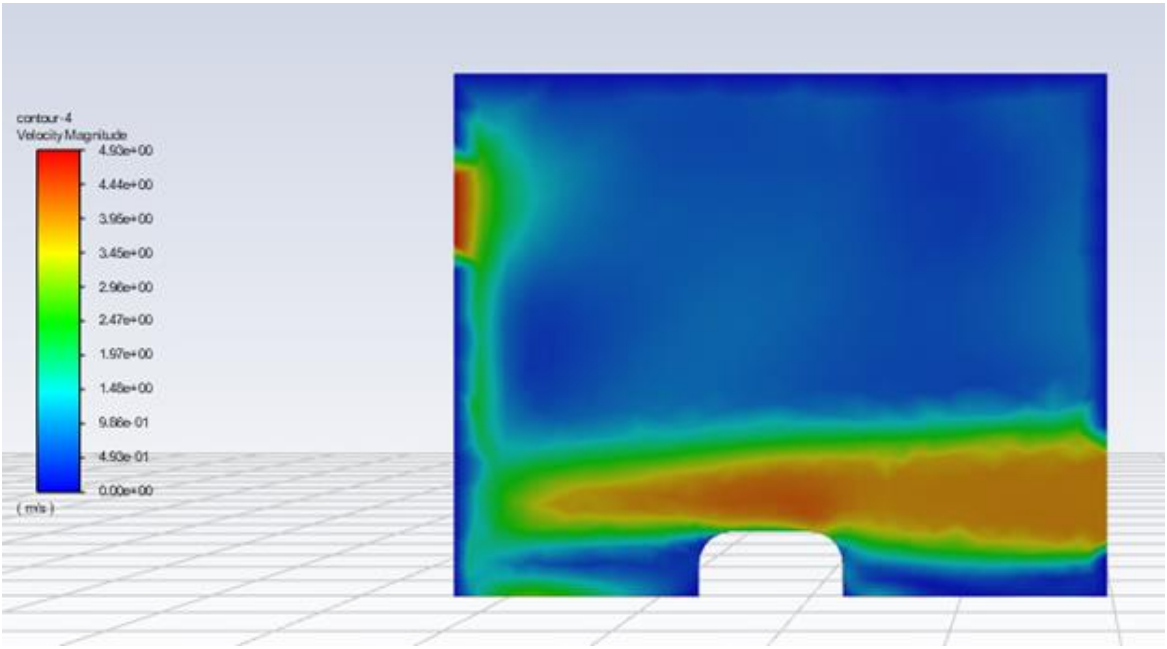

Figure B8. Velocity Distribution from Transient Simulation

APPENDIX C: Phase Change Meat Model

Final Run (Run Time: 14 min, Time Step: 0.5 s, Heat Flux: 333.33 W/m2, Inlet: 8m/s, Ambient: 300 K)

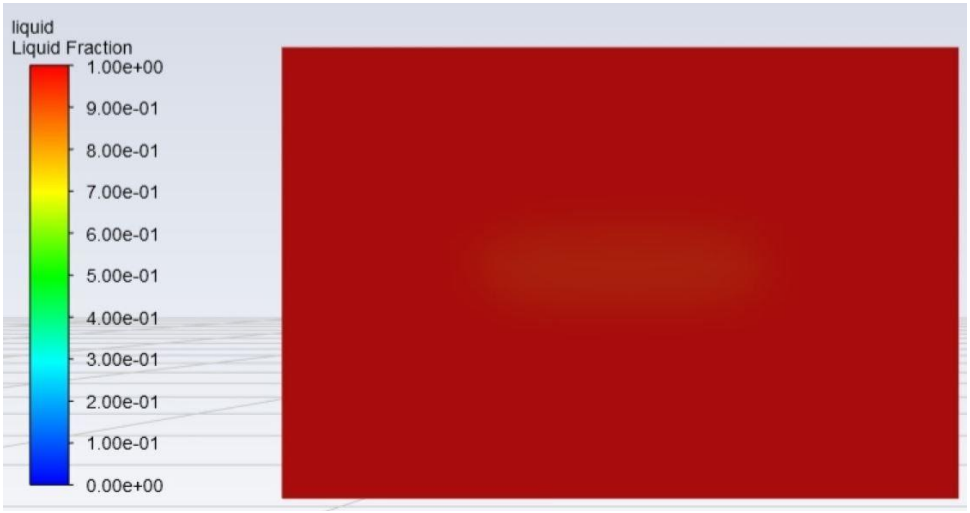

Figure C1: Liquid Fraction after 10.5 minutes

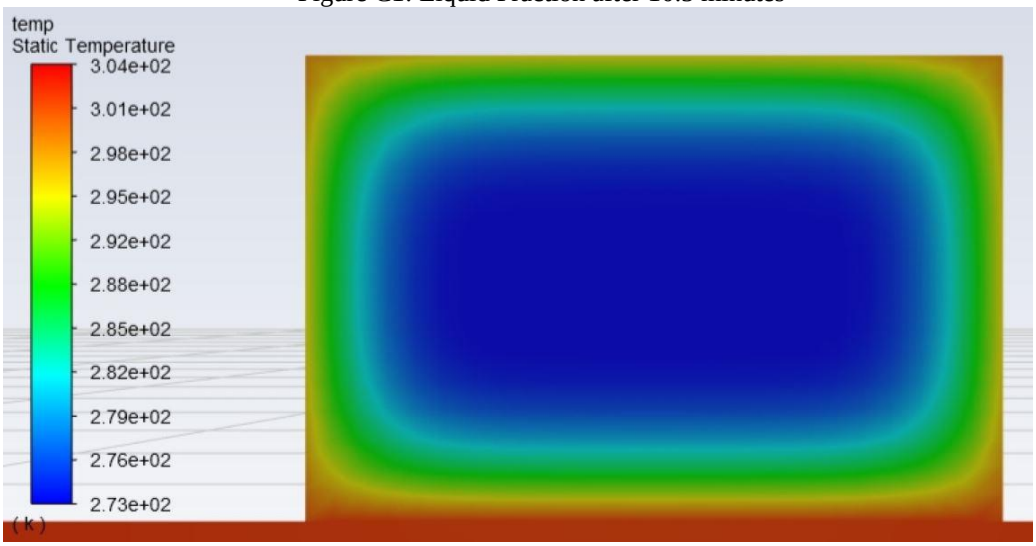

Figure C2: Temperature Distribution after 10.5 minutes

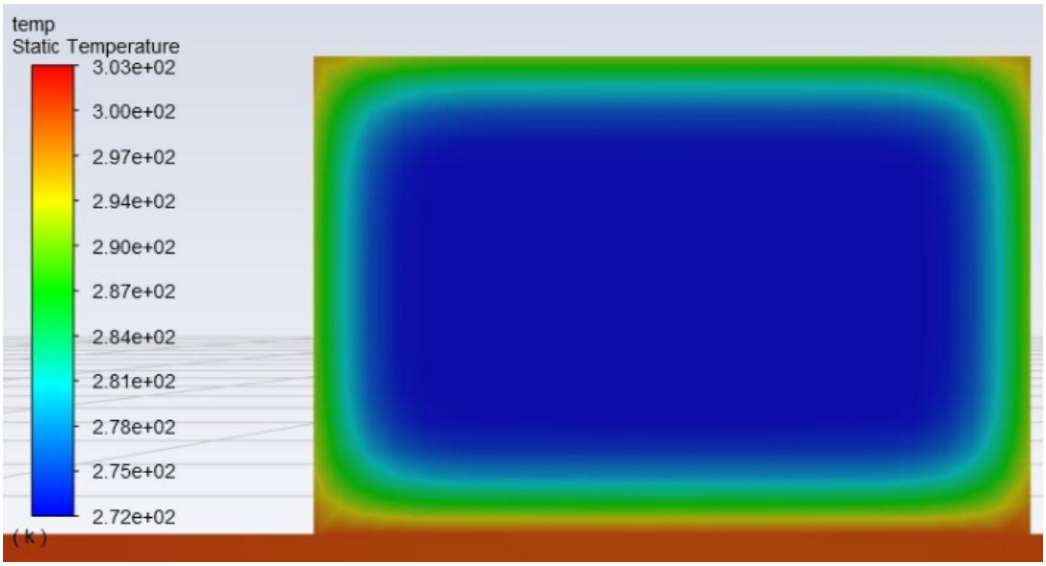

Figure C3: -1°C after 7.125 minutes

APPENDIX D: Sample of Meat Block Geometries

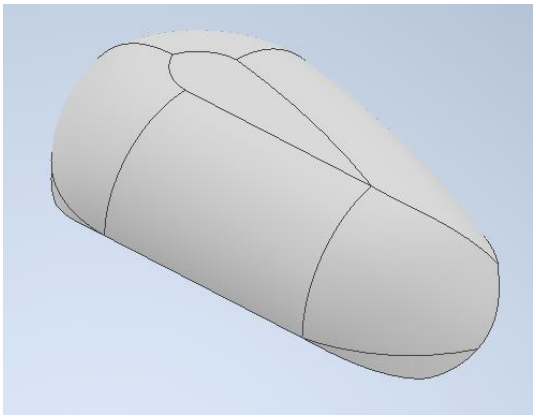

Figure D1: Rejected Meat Form (Chicken Breasted)

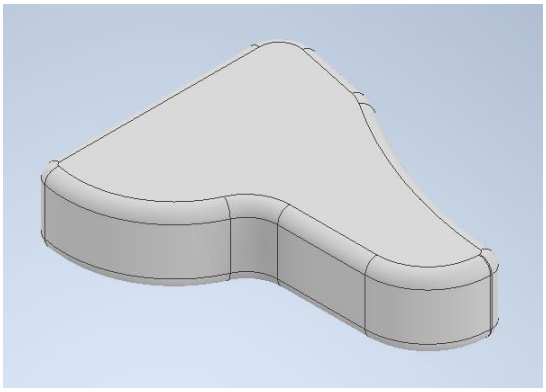

Figure D2: Rejected Meat Form (Beef Steak)

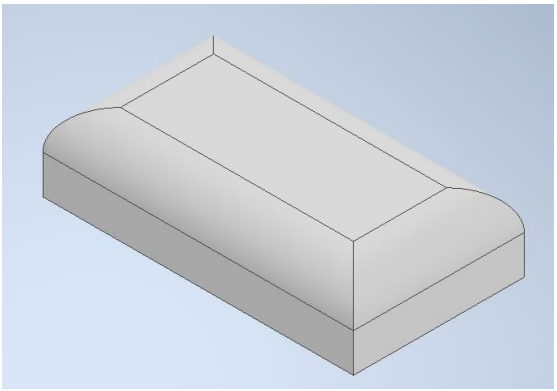

Figure D3: Chosen Meat Form (Symmetrical Slab)